Sensors & Actuators: A. Physical 372 (2024) 115376

Contents lists available at ScienceDirect

Sensors and Actuators: A. Physical

journal homepage: www.journals.elsevier.com/sensors-and-actuators-a-physical

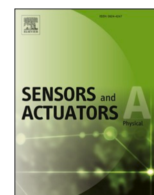

Impact of alternating precursor supply and gas flow on the LPCVD growth behavior of polycrystalline 3C-SiC thin films on Si

Philipp Moll [a,*], Georg Pfusterschmied [a], Sabine Schwarz [b], Michael Stöger-Pollach [b], Ulrich Schmid [a]

[a] Institute of Sensor and Actuator Systems, TU Wien, Austria
[b] Service Unit of University Service Centre for Transmission Electron Microscopy, TU Wien, Austria

ARTICLE INFO

Keywords:
3C-SiC
Alternating supply deposition
LPCVD
Silicon carbide

ABSTRACT

In this paper, we will provide information on the growth mechanism of 3C-SiC using alternating supply deposition (ASD). SiH_4 and C_3H_8 were introduced successively in a low-pressure chemical vapor deposition (LPCVD) system at 1000 °C, forming a stoichiometric polycrystalline 3C-SiC thin film on Si substrates. We demonstrate the influence of different gas flow rates on thin film properties. In detail, altering the flow rates of the precursors and the carrier gas resulted in changes of the growth rate, the surface roughness, the crystal growth mechanisms as well as the crystal quality. Hydrogen inhibition and passivation are proposed to be the main effects influencing the growth behavior of ASD thin films. Applying ASD to grow 3C-SiC thin films with precursors from low to high flow rates resulted in a transition of different growth mechanisms influencing the surface roughness and grain size. Furthermore, we could prove that ASD is a cyclic step-by-step carbon-assisted redistribution of a prior deposited silicon film. This is shown by contact angle measurements of three differently terminated surfaces during the specific phases of one ASD cycle. High resolution transmission electron microscopy (HRTEM) analysis showed a continuous and homogenous thin film and confirmed the absence of silicon- or carbon-rich layers. ASD enables 3C-SiC thin films with customized properties for tailored micro electromechanical system (MEMS) applications.

1. Introduction

Since 30 years silicon carbide (SiC) is one of the most promising electronic as well as structural material for both advanced microelectronic and microelectromechanical system (MEMS) applications [1–7]. This is due to its outstanding properties especially for harsh environmental applications compared to standard silicon (Si) solutions [8]. SiC is a high-performance material for devices or circuits designed to operate under high-power, high-temperature and/or chemically aggressive conditions. In addition, SiC has the beneficial property of a large acoustic velocity, which gives the opportunity to use it the fields of micro- and nanomechanical resonators [9]. SiC is also known for its wide bandgap ranging from 2.29 eV to 3.3 eV, depending on the polytype [5,10]. However, only the 3 C polytype (also called β-SiC) has a pure cubic lattice structure.

The integration of 3C-SiC thin films in a silicon fabrication process is well reported in literature [4,7,9,11–18]. Besides the crystallographic lattice aspects, silicon has a melting point of 1410 °C, which is why only the synthetization of 3C-SiC can be achieved on silicon substrates, since all other polytypes require higher process temperatures [19,20]. Depending on the deposition parameters heteroepitaxial single crystalline [9,11,21–24] as well as polycrystalline 3C-SiC layers can be formed on Si substrates [1,4,7,13–16,25–27]. Many MEMS devices, however, are not restricted to high-quality single-crystal SiC, as required in electronic devices. Therefore, polycrystalline SiC is also well-suited as a structural material, offering high hardness (3C-SiC: 33.5 GPa; Si: 12.6 GPa; poly Si: 11 GPa [28,29]), mechanical strength (3C-SiC: ~350 GPa; Si: 165 GPa; poly Si: 160 GPa [30–32]) and chemical inertness to most standard chemicals, even when operated at elevated temperatures. A straightforward and safe deposition technique is provided by low-pressure chemical vapor deposition (LPCVD) at moderate temperatures in the range between 800 °C – 1200 °C [1,14,23]. Besides Si substrates LPCVD can be used for poly 3C-SiC thin film deposition on other substrates such as silicon nitride (Si_3N_4) [33], silicon dioxide

* Correspondence to: TU Wien, Institute of Sensors and Actuator Systems, Austria
E-mail address: philipp.moll@tuwien.ac.at (P. Moll).

https://doi.org/10.1016/j.sna.2024.115376
Received 22 January 2024; Received in revised form 14 March 2024; Accepted 11 April 2024
Available online 16 April 2024
0924-4247/© 2024 The Author(s). Published by Elsevier B.V. This is an open access article under the CC BY license (http://creativecommons.org/licenses/by/4.0/).

(SiO_2) [4,25,34–36] or diamond [37]. In general, studies distinguish between single- [1,7,15,26,27,38] and dual-precursor deposition [2,4, 11,13,14,16,25,39–42]. Both techniques can be employed in either continuous or pulsed CVD processes. The latter involves the intermittent delivery of precursor gases into the reaction chamber, in contrast to continuous flow CVD, also known as simultaneous supply deposition (SSD), where gases are continuously supplied. In pulsed CVD the gas flow is alternated between on and off periods. An advanced form of pulsed CVD, known as alternating supply deposition (ASD), introduces two or more precursor gases sequentially into the reaction chamber [24, 43–46]. Most prominently used in dual precursor depositions is SSD, because of its simplicity and stability. However, we decided to use the ASD technique, because ASD claims to provide thin films with smaller full width at half maximum (FWHM) of X-ray diffraction (XRD) rocking curves, smoother surfaces and enables the possibility to synthesize even monocrystalline thin films at process temperatures below 1100 °C, indicating a higher crystal quality compared to SSD deposited thin films [45]. Furthermore, ASD also gives the opportunity of a more versatile deposition scheme, which allows a precise tailoring of the resulting thin film characteristics such as thermal [47], structural, mechanical and electrical properties. However, the process of SiC crystal growth based on ASD is still not fully understood. As a consequence, different concepts or theories on film formation are available [43].

In the Results chapter we investigate the influence of the process gas flows on thin film properties such and give a detailed description of the SiC deposition scheme. Furthermore, we draft a basic crystal growth mechanism of poly 3C-SiC when applying ASD using further experimental techniques such as contact angle (CA) measurements. To the best of the authors' knowledge the impact of controlled altering of precursor gas supply for poly 3C-SiC thin film synthetization with ASD has not been reported yet.

2. Experimental details

For the deposition of polycrystalline 3C-SiC thin films we used 4 in. n-type Si <100> wafers with a bulk resistivity of 50 Ω·cm. As LPCVD reactor we used an Easy Tube 3000EXT industrial quartz oven from FirstNano. A brief description and a schematic illustration will be provided in the supplemental materials. The tailored deposition process in our LPCVD system splits up in three steps consisting of an *in-situ* hydrogen (H_2) cleaning step with 5000 sccm H_2 for 10 min at 1000 °C and atmospheric pressure, followed by a carbonization step, which acts as an intermediate buffer to overcome the lattice mismatch of ~20 % [19,48] and passivates the attackable Si surface from hydrogen etching. While the cleaning step with H_2 is straightforward, the carbonization step comes with many challenges [22,24,45,49–54]. Hereby, we used an optimized fast carbonization step, whereby the furnace ramps up from 900 °C to 1085 °C with 9.25 °C/min, 100 sccm of propane (C_3H_8) and 1000 sccm of H_2 at 20 torr. A subsequent dwelling at the latter conditions for 5.5 min finishes the carbonization step. The third step of the fabrication process consists of introducing the process gases into the reaction chamber. Specifically, we used pure silane (SiH_4) and pure C_3H_8 as precursor gases in an alternating regime. H_2 was implemented as carrier gas to support a sufficient flow regime [7,8]. Fig. 1 illustrates the basic gas flow concept of the precursor and carrier gases of one ASD cycle.

The first part of the presented results will provide information of the changing thin film characteristics depending on five precursor flow rate combinations and two different carrier gas flow rates Ψ_{low} and Ψ_{high}. The specific values for the flow rates can be found in Fig. 2. The ratio for the precursor gases of SiH_4/C_3H_8 was set to 1/4, with timeslots for SiH_4 (t_1 – t_2) of 7 s, 3.5 s for C_3H_8 (t_3 – t_4) and 5 s for the pump-out step. The process temperature was measured right under the center of the 4-inch wafer and held constant at 1000 °C. The chamber back pressure was set at 0.32 ± 0.02 torr during deposition.

To start, we determined the growth per cycle for Ψ_{high} by depositing

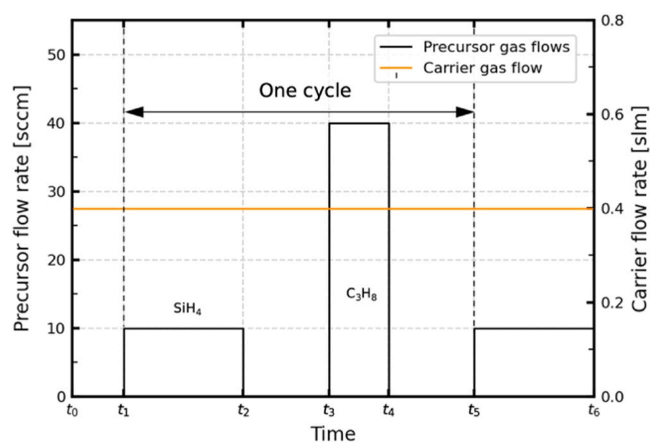

Fig. 1. Schematic illustration of temporal gas introduction within the ASD scheme for poly 3C-SiC thin film synthetization.

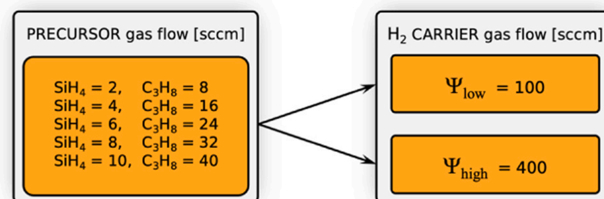

Fig. 2. Five different precursor gas combinations were chosen to investigate the change in 3C-SiC thin film properties. All precursor gas flow combinations were deposited with two different carrier gas flows.

thin films with 800 ASD cycles with each precursor gas species. With the calculated growth per cycle for each precursor gas flow, we aimed in a second step for a thickness of 400 nm for all thin films. To investigate the growth behavior during the ASD process, we performed five additional depositions with SiH_4 = 10 sccm, C_3H_8 = 40 sccm and H_2 = 400 sccm (also Ψ_A) with 10, 30, 60, 90 and 120 ASD cycles. The layer thickness was determined in the middle of the wafer by utilizing a Filmetrics F20-UVX thin film analyzer with wavelengths in the range from 600 nm to 1600 nm. In a second approach these results were confirmed by cross-sectional Scanning electron microscopy (SEM) measurements, where the thin film thickness was determined from the silicon edge, thus including the carbonization layer. Hereby, a Hitachi SU8030 was used with 4 kV acceleration voltage. For the characterization of the carbonization layer cross-sectional transmission electron microscopy (TEM) measurements in standard and high resolution (HRTEM) configuration were taken with a TECNAI F20 operating with an acceleration voltage of 200 kV. Also, electron diffraction patterns were recorded at interface-near regions. Electron energy loss spectroscopy (EELS) measurements were performed with a GATAN GIF Tridiem energy filter and spectrometer. For this purpose, TEM was operated in scanning mode (scanning TEM - STEM) and the electron probe was focused and scanned through the thinned specimen.

For chemical analysis we applied X-ray photoelectron spectroscopy (XPS) depth profiling. These measurements were done with a SPECS XP-spectrometer equipped with a monochromatic Al-Kα X-ray source and a hemispherical WAL-150 analyzer. X-ray diffraction (XRD) measurements were performed to identify the crystallographic phases present in the thin films. This was done with a Malvern PANalytical X′pert PRO X-ray powder diffractometer and carried out with Cu-Kα radiation operating at 45 kV and a current of 40 mA. The wavelengths of the X-rays was 1.540598 Å for $K\alpha_1$ and 1.544426 Å for $K\alpha_2$. The Bragg Brentano measurements were carried out from $2\theta = 15°$ to 90 ° and the range for

the rocking curves was set from 34 ° – 38 °, since the most prominent 3C-SiC <111> peak was expected at around 36 °. To make a quantitative statement of the preferred crystallographic growth orientation, we calculated the texture coefficient (TC) according to [55] with

$$TC_{(hkl)} = \frac{I_{m(hkl)}/I_{0(hkl)}}{\left(\frac{1}{n}\right)\sum\left[I_{m(hkl)}/I_{0(hkl)}\right]}. \quad (1)$$

In this context, *(hkl)* represents the growth plane under consideration, I_m stands for the normalized measured intensity after subtracting the background intensity, I_0 represents the intensity of a randomly oriented polycrystalline sample obtained from a Powder Diffraction File (PDF) card and *n* denotes the number of planes being evaluated. The PDF card used in this work for 3 C-SiC was #00–029–1129 and the investigated planes to calculate the TC were (111), (200), (220), (311) and (222), hence *n* was 5. For the determination of the surface roughness and grain size of our thin films we performed atomic force microscopy (AFM) measurements with a Bruker Dimension Edge atomic force microscope in tapping mode, with a NHCV-tip (spring constant ~40 N/m) and evaluated the RMS roughness from the measurements with a scan size of 3×3 μm^2.

The second part focuses on the investigation of the ASD growth behavior. Therefore, three Ψ_A thin film depositions were terminated at different stages during a typical ASD cycle (see Fig. 1). The first sample worked as reference and was terminated after a typical $SiH_4 \rightarrow C_3H_8$ sequence. The second sample was silicon-terminated and ended after a $SiH_4 \rightarrow C_3H_8 \rightarrow SiH_4$ sequence. The third sample was carbon-terminated and ended after one additional propane sequence with $SiH_4 \rightarrow C_3H_8 \rightarrow C_3H_8$. The CA of each sample was measured right after deposition and after two days. Using the sessile droplet method with a Krüss DSA30S drop shape analyzer, the CA was measured with 2 µl droplets.

3. Results and discussion

3.1. Thin film characterization

The growth per cycle of the different 3C-SiC thin films was determined as a function of the process gas flow rates, as illustrated in Fig. 3. It can be seen that for all precursor flow rates the growth per cycle for Ψ_{low} is larger, than for Ψ_{high}. Even if more precursor gases are provided, less SiC is formed with Ψ_{high} compared to depositions with Ψ_{low}. This stands in contrast to classic CVD theory, if a higher carrier flow rate for the same amount of precursor gases is applied, also the growth rate is intended to increase. From this result we conclude, that during depositions with higher carrier gas flow rates, the effective Si thickness is reduced due to a higher exposure to H_2. Beside other possibilities, three main effects are reported for polysilicon explaining this result. First, hydrogen inhibition [56–58], whereas the H_2 interacts with the Si surface, affecting its reactivity and leading to changes in the deposition process. Hereby the growth rate is inversely proportional to the hydrogen partial pressure. The second vital mechanism for an inhibited growth rate of 3C-SiC with higher H_2 flow rates is hydrogen passivation [59].

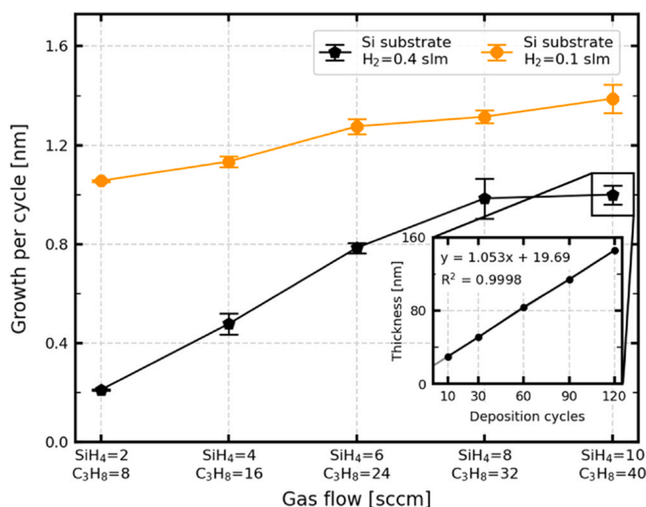

Fig. 3. Growth per cycle of polycrystalline 3C-SiC thin films deposited with increasing precursor gas supply and for two different carrier gas flows on Si. The insert shows the dependence of the overall film thickness as a function of total number of deposition cycles. The layer thickness was measured in the middle of the sample. The inserted lines serve as guide to the eye.

This involves a saturating coverage of surface defects or Si dangling bonds with hydrogen atoms. If these surface sites are essential for the adsorption and incorporation of C precursors, the passivation can hinder the adsorption process and as a consequence reduce the deposition rate. Especially if the hydrogen concentration is high, it might interfere with the availability of Si and C precursors for the SiC deposition, thereby decreasing the overall deposition rate. And third, hydrogen thermal etching [60], where the interaction of hydrogen gas with the Si surface leads to the removal of silicon atoms and the formation of volatile silicon hydrides (SiH_x) All three effects can happen simultaneously, however, further measurements to investigate the exact mechanisms taking place are recommended.

Next, the increase of the precursor flow rates led to an almost linear increase of the growth per cycle for Ψ_{low} depositions (yellow curve). For Ψ_{high} saturation of the initially increasing growth per cycle was observed, when increasing the precursor flow rates above a threshold of 8 sccm for SiH_4 and 32 sccm for C_3H_8. For clarification an additional deposition with flow rates of 20 sccm SiH_4 and 80 sccm C_3H_8 achieved also a growth per cycle of ~1 nm per cycle. This confirmed the assumption, that a reaction limited regime saturates the growth per cycle of 3C-SiC, as enough precursor gases are provided, but no further increasing of the growth per cycle was measured. In contrast to those samples synthesized with Ψ_{high}, the increase of the precursor values, had less impact on the growth per cycle for Ψ_{low} depositions. Overall, a layer thickness deviation of 5 ± 2.5 % was achieved in the inner 3.5 in. of the investigated samples. In the regions close to the edge deviations up to 50 % were observed.

The insert of Fig. 3 illustrates an increase of the thin film thickness (including the carbonization layer) as a function of ASD cycles for Ψ_A depositions. With a linear regression of $R^2 = 0.9998$ a highly linear growth regime is confirmed, whereby after only 10 ASD cycles we achieved homogeneous and continuous thin films. The intercept with the y-axis of ~19.7 nm derived from the linear equation represents the thickness of the carbonization layer. A TEM analysis of the poly 3 C-SiC/Si interface in cross-sectional view confirms the thickness of the carbonization layer with about ~20 nm (see Fig. 4). The crystallinity of the interface-near regions was determined with electron diffraction patterns, as illustrated in Fig. 4 c). For the 3 C-SiC thin film a polycrystalline diffraction pattern was measured, whereas the carbonization layer was found to be amorphous. For the Si substrate a single crystalline diffraction pattern was recorded.

EELS spectra were recorded along the line shown in Fig. 4 b. The corresponding intensity detected during a high-angular annular dark-field (HAADF) line scan acquisition is shown in Fig. 5 a. It can be clearly distinguished between the Si substrate, a SiC capping layer of ~5 nm thickness, an amorphous carbon layer with strongly varying thicknesses around 15 nm and the SiC layer on top. In every position of the beam an EELS spectrum was recorded including the Si-L edge at 99 eV energy loss and the C-K edge at 284 eV energy loss. The fine structure of the ionization edge is related to the electronic state of the probed atoms. From Fig. 5b it is obvious that the amorphous carbon layer does not contain any silicon. From Fig. 5c it can be derived that the Si substrate does not contain any carbon. The energy loss near edge structure (ELNES), which is the fine structure of the ionization edge,

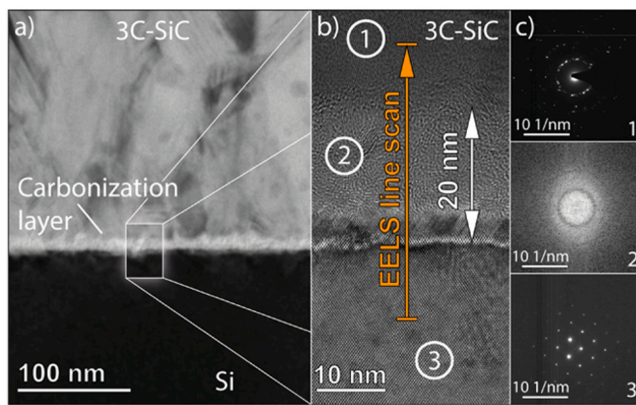

Fig. 4. A TEM analysis of the interface region of poly 3C-SiC grown on silicon is provided in a). A ~20 nm thin carbonization layer was determined in the illustrated area of b). Electron diffraction patterns were evaluated in c), where a poly crystalline pattern on cubic SiC can be seen in 1, the amorphous nature of the carbonization layer is shown in 2 and a perfect Si lattice crystal was measured in 3.

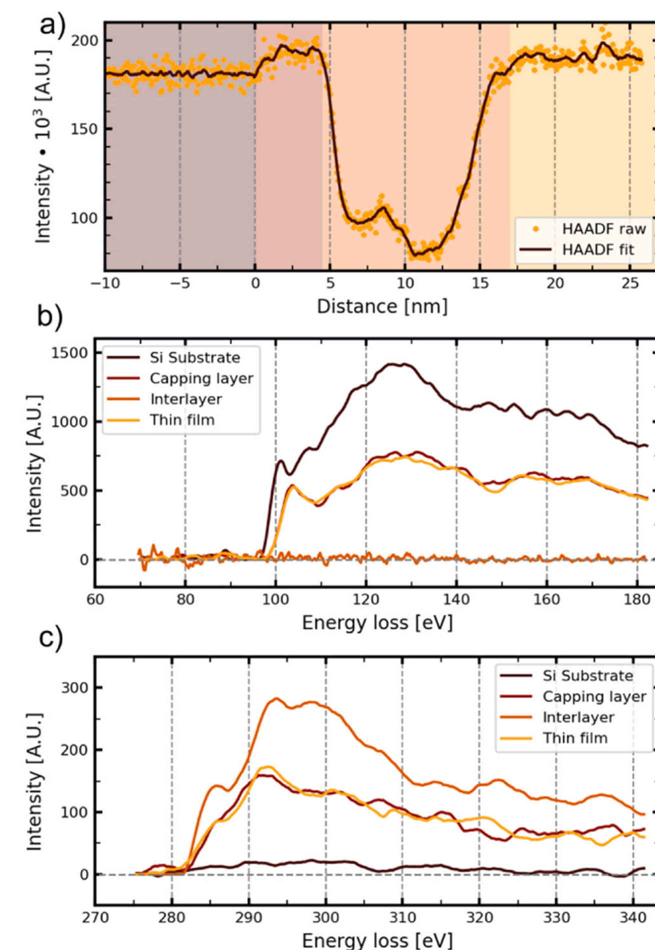

Fig. 5. EELS results of the interface region. HAADF measurements depict various regions throughout the line scan, as illustrated in a). In b) and c) the EELS spectrum around the Si-L edge at 99 eV and the C-K edge at 284 eV is illustrated.

proves that the capping layer is pure SiC. The ELNES of the Si-L edge, as well as the one of the C-K edge of both, the capping layer and the SiC layer on top, are identical. Both Si-L edges show the characteristic chemical shift compared to pure silicon.

In Fig. 6, a chemical analysis with XPS depth-profiling is presented. In the poly 3C-SiC layer, a stochiometric composition of silicon and carbon is confirmed. This finding is consistent through the entire thin film also including the surface, where an increase of oxygen was

measured indicating the formation of a native oxide. Even more, the thickness of the carbonization layer is estimated to about 20 nm before reaching into the silicon substrate.

Besides the fact that all three independent measurement techniques lead to similar results for the carbonization layer thickness, these values are also in excellent agreement with data provided by literature ranging from 5 nm to 25 nm [1,45,50]. Both thin films from Fig. 4 and Fig. 6 were deposited with Ψ_A.

The results from the XRD measurements can be seen in Fig. 7a) The most prominent peak at 35.78 ° can be assigned to the 3C-SiC <111> direction. Together with the other peaks detected at 41.48 ° and 56.29 °, which can be assigned to the <200> and <220> direction, respectively, the typical diffraction patterns indicate, that all thin films consist of poly 3C-SiC [61,62]. However, the <111> peak was expected at 35.6 °[62]. The difference of 0.18 ° refers to a change in the lattice plane distance of $\Delta d_{111} = 0.0116$ Å, originated from low-angle grain boundaries resulting in intrinsic compressive strain.

The TC calculations suggest that the 3C-SiC thin films have no preferred growth orientation [55], as the results can be found around 1, illustrated in Fig. 7b). Nevertheless, small differences of the TC between Ψ_{low} and Ψ_{high} are visible, especially for <110>.

Literature offers two main explanations for the absence of a preferred crystal orientation or if present, its deviation from the seed crystal provided by the substrate. First, differences in the carbonization layer [63] or second as a combination of deposition parameters [55,63,64]. The reason why the <111> peak shows the highest intensity is because of the low free surface energy of <111> facets, that form <111> SiC, even though the substrate is <100> orientated or amorphous [4]. In literature this is a known effect for 3C-SiC depositions [42,63,65,66], although the <110> direction features an even lower surface energy of 3.4 J/m^2 compared to 4.2 J/m^2 of the <111> direction [67]. Nishiguchi *et al.* investigated SiC growth on <110> Si, where the thin films were also most prominently oriented in the <111> direction [64]. This was explained by the density of aligned atoms per unit. The density of <111> 3C-SiC on <110> Si is four times higher, than <110> 3C-SiC on <110> Si, thus causing the favored formation of <111> 3C-SiC.

The rocking curves revealed FWHM values between 1.112 ° and 1.302 °. Literature reports for high quality poly 3C-SiC thin films FWHM values from 1.4 ° to 1 ° [43], while epitaxial grown 3C-SiC-on-Si can achieve values as low as 0.25 ° at 400 nm film thickness [24]. The two lowest FWHM values came from the depositions of Ψ_{low} paired with the lowest precursor flow rate (1.138 ° FWHM) and Ψ_{high} with the highest precursor flow rate (1.112 ° FWHM). This finding demonstrates, that the ratio between the precursor and the carrier flow rate is most important for high quality SiC layer synthetization. This could also be explained by the hydrogen inhibition-effect, since only matching precursor and carrier flow rates (high precursor - high carrier and low precursor low -

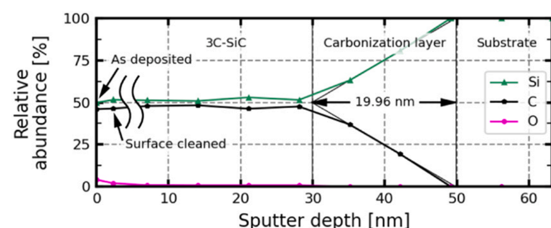

Fig. 6. XPS depth profiling showing the local distribution of Si, C and O concentrations across the film thickness including the SiC-Si interface. With a depth resolution of ~7 nm, a thickness of ~20 nm was measured for the carbonization layer.

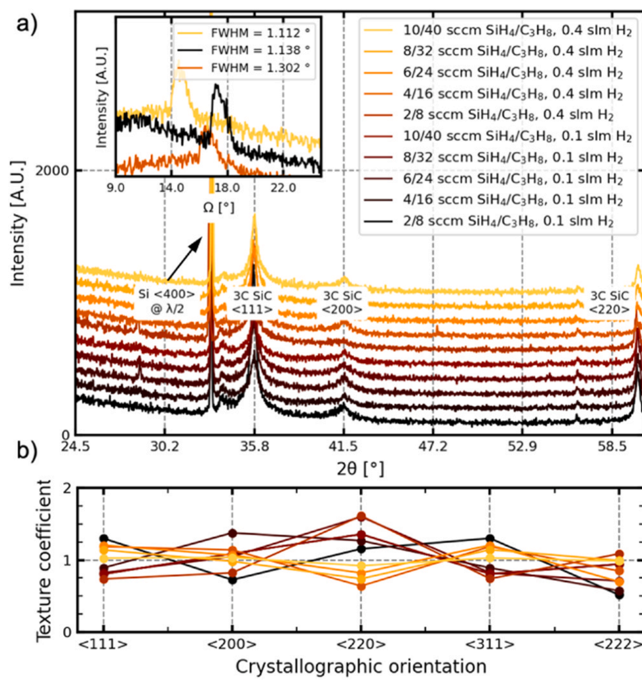

Fig. 7. In a) the XRD measurements of thin films investigated in this study showing typical features of polycrystalline 3C-SiC 2θ diffraction patterns. Most prominent is the <111> peak of 3C-SiC at 35.79 °. The TC for each crystallographic orientation is illustrated in b). Note: the legend of a) also applies for the insert, as well as for b).

carrier flow) achieved superior results in FWHM values.

For the surface roughness analyses all samples were measured with AFM. Representative surface patterns are illustrated in Fig. 8a and b, which are comparable to what can be found in literature [2,4,14]. The roughness results were set in relation with the corresponding layer thickness of each sample and are illustrated in Fig. 8c and d. Two major tendencies can be derived from the surface roughness measurements. For Ψ_{high} a descending trend of the roughness for constant layer thicknesses of 400 nm ± 5 % can be observed. This trend is also represented in the roughness/thickness ratio. On the other hand, an inverted trend of the roughness/thickness ratio for Ψ_{low} was observed.

Although this study did not pursue the target to achieve 3C-SiC thin films with a minimal surface roughness, we achieved smooth surfaces with an RMS roughness under 7 nm. In literature this is already considered as mirror-like [14], whereas roughness values of poly 3C-SiC down to 3 nm at ~400 nm are achievable [43], while also values of 60 nm and above can be found [68].

The second important finding showed different dependencies of the surface roughness from the layer thickness. Table 1 provides results from the surface roughness measurements from the lowest and highest precursor flow rates of both, of Ψ_{low} and Ψ_{high}. Hereby is d_{layer} the layer thickness and R_{RMS} the root mean square roughness. For the lowest precursor flow rates of 2 sccm for SiH_4 and 8 sccm for C_3H_8 an almost independency of the surface roughness from the layer thickness is shown. This means, that the SiC grains maintain their size independently from the layer thickness. Thus, a columnar growth behavior is proposed

For the highest precursor flow rates of 10 sccm for SiH_4 and 40 sccm for C_3H_8, however, a strong linear dependency of the roughness with respect to the layer thickness is detected, reflected in almost constant values of the roughness/thickness ratio (see Table 1). Because of these results we propose a change of the growth regime, where the crystals grow with a linear dependency with the layer thickness. Thus, a triangular growth behavior is intended. This leads to the conclusion of different crystal growth regimes depending on the precursor flow rates. Additionally, it is worth mentioning that this behavior was found to be independent of the carrier flow rates.

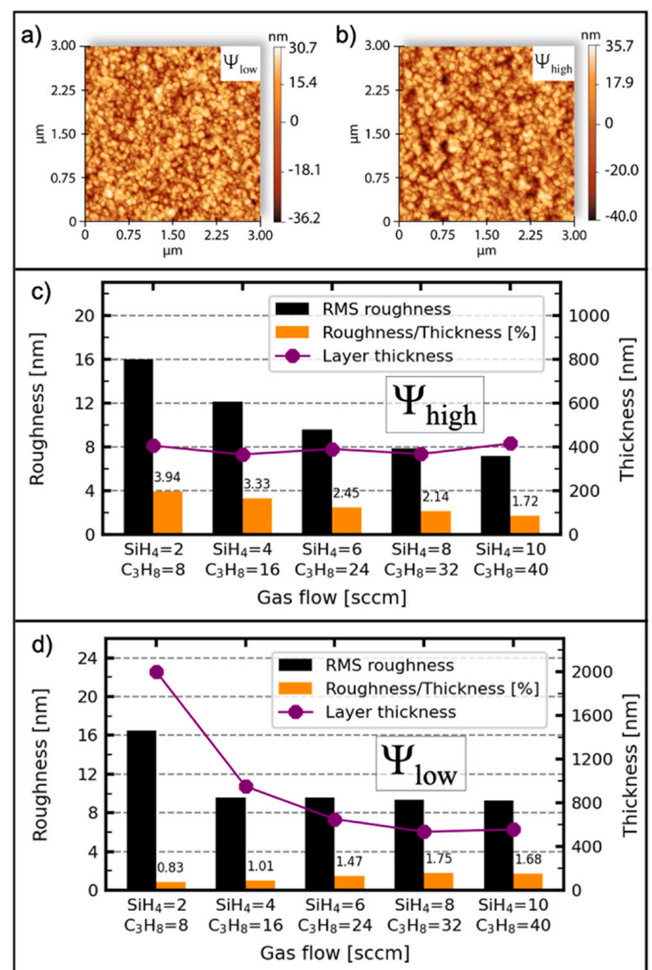

Fig. 8. In a) and b) representative AFM pictures are presented, from depositions with the same precursor flow rates of SiH_4 = 10 sccm and C_3H_8 = 40 sccm with Ψ_{low} and Ψ_{high}, respectively. A comparison of the surface roughness values depending on the precursor and the carrier gas flow can be seen in the lower section of the figure. In c) the results of depositions on Si with Ψ_{high} can be seen, while in b) results for Ψ_{low} is shown.

Table 1
Decreasing roughness per thickness values for the lowest precursor gas flow stand in contrast to almost constant values for the highest precursor gas flow, indicating different growth mechanisms.

Lowest precursor gas flow SiH_4 = 2 sccm, C_3H_8 = 8 sccm			**Highest precursor gas flow** SiH_4 = 10 sccm, C_3H_8 = 40 sccm		
d_{layer} [nm]	R_{RMS} [nm]	R_{RMS} /d_{layer} [%]	d_{layer} [nm]	R_{RMS} [nm]	R_{RMS} /d_{layer} [%]
169	15.02	8.89	225	3.89	1.73
405	15.97	3.94	415	7.13	1.72
842	16.43	1.95	555	9.30	1.68
2000	16.52	0.83	800	14.12	1.77

3.2. Growth process

In this section we will present information of the actual growth mechanisms of ASD thin films. Wang *et al.* and Huang *et al.* proposed concepts of the ASD thin film growth [43,46]. The process for growing smooth SiC layers basically consists of three parts:

- Deposition of Si

- Carbon diffusion in Si
- Redistribution of the Si and C atoms

Thus, the proposed growth mechanism is a repeated step by step deposition of Si atoms and the subsequent carbon-assisted redistribution forming ultimately SiC. The concept is illustrated in Fig. 9. However, this concept has not been proved yet, which means the actual growth mechanism could be similar to SSD.

The CA angle measurements presented in Fig. 10 give information about hydrophilicity of the differently terminated surfaces and eventually leads to a conclusion of the ASD crystal growth. Strong differences of the CA of the three surfaces can be seen. At first, the initial CA at 0 s and directly after deposition (CA_{AD}) will be taken into account.

From the orange curve a typical $SiH_4 \rightarrow C_3H_8$ terminated ASD cycle with a CA_{AD} of 37 ° is determined. Such thin films were already confirmed as stoichiometric poly 3C-SiC layers by XPS and XRD measurements. Now, by looking at the silicon-terminated surface ($SiH_4 \rightarrow C_3H_8 \rightarrow SiH_4$, purple curve) a decreased CA_{AD} of only 26 ° is observed. Thus, during every single ASD cycle an ultra-thin layer (<1 nm) of silicon is deposited [69,70]. This finding, in fact, ensures that 3C-SiC is not constantly formed at the surface like in SSD. In a standard ASD cycle the next sequence introduces C_3H_8 into the reaction chamber and leads at the surface to a carbon-assisted redistribution (also called carbonization) of the uppermost Si layer resulting in 3C-SiC formation.

On the other hand, the $SiH_4 \rightarrow C_3H_8 \rightarrow C_3H_8$ terminated surface (red curve) shows an increased CA_{AD} of 54 °. This provides information of how crucial the deposition times and flow rates are when applying ASD. The increased CA_{AD} represents a carbon-terminated surface, which means that too much C-precursor was introduced. After the silicon is all consumed during the redistribution and forming SiC, the additional C_3H_8 was adsorbed on the surface forming a thin carbon layer. Hence, if too much C-precursor is used during a standard ASD process a repetitive stacked microstructure of SiC and C layers would result.

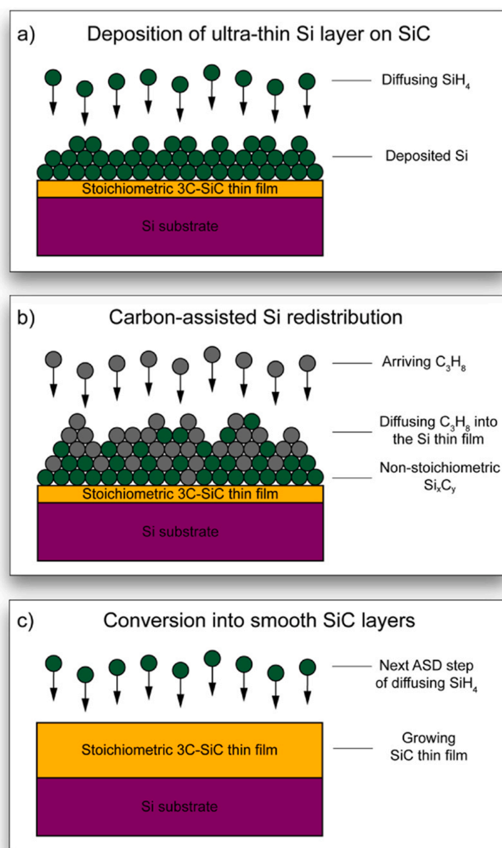

Fig. 9. Schematic step-by-step illustration of one ASD cycle. Each cycle starts with the deposition of an ultra-thin layer of silicon (a), which is not directly converted into SiC. In the next sequence C_3H_8 is introduced and reacts with the present silicon layer. In b) the carbon-assisted redistribution of the silicon atoms with can be seen, which ultimately leads to a smooth SiC thin film (c).

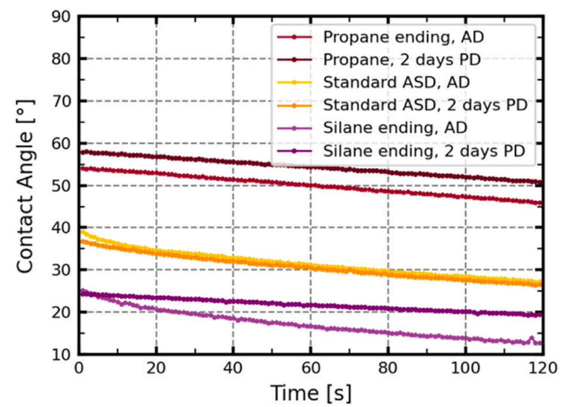

Fig. 10. Contact angle measurements over 120 s on three differently terminated ASD cycles. The samples were each measured two times, once directly after deposition (AD) and a second time two days post deposition (PD) to reveal oxidation processes on the three different surfaces. Every measurement on each sample was carried out four times on different locations on the wafer.

More information is revealed, when the CA of two days post deposition (CA_{PD}) in air is compared to CA_{AD}, over the period of 120 s. The major effect for the decrease of the CA over time is a result due to the evaporation of the water droplet. This leads to a decrease in volume of the droplet and since the contact edges can be assumed as clamped, the CA decreases [71]. The samples were stored in air and therefore start to form a native oxide layer [72,73]. SiC features a lower oxidation rate compared to Si [72–74], which is why only minor changes of the CA are observed (orange curves). Pure Si (purple curves) on the other hand has a chemically unstable surface [75], resulting in a lower CA_{AD} and a faster decrease of CA_{AD} from 0 s to 120 s compared to all other measurement cycles.

After oxidation, however, the oxidized Si surface (SiO_2) is chemically more stable [75] resulting in a slower decrease over time of CA_{AD} and a higher CA_{PD} after 120 s The increase of the CA_{PD} of the oxidized carbon-terminated surface can also be observed (red curves). This can be explained by the faster oxidation rate of C-rich SiC faces [76,77]. Ultimately, the specific oxidation behavior of the different elements proves that the three investigated surfaces are differently terminated, thus, once again indicating that ASD is a process consisting of sequential silicon deposition and its subsequent carbonization. Finally, a HRTEM analysis of the 3C-SiC/Si interface provided in Fig. 11 shows a continuous 3C-SiC thin film, where no Si- or C-rich intermediate layers were detected, confirming the CA measurements.

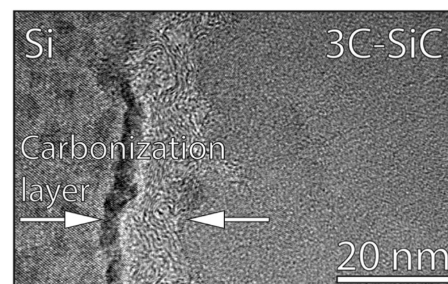

Fig. 11. HRTEM recording of the 3C-SiC/Si interface. The ~20 nm thick carbonization layer can be clearly distinguished from the Si substrate and the 3C-SiC thin film. No Si- or C-rich layers can be observed in the thin film.

4. Conclusions

In this study we demonstrated the deposition of polycrystalline 3C-SiC thin films on Si with ASD. Altering the precursor flow rates of SiH_4 and C_3H_8 as well as the H_2 carrier flow rate impacts the thin film properties. A higher growth per cycle was detected for Ψ_{low} for all precursor flow rates, caused by the effects of hydrogen inhibition and passivation. The carbonization layer thickness was determined by three methods with ~20 nm. XPS and XRD measurements revealed that all thin films were stoichiometric and most prominently orientated in the <111> plane, regardless of the <100> orientation of the Si substrate. Low FWHM values of 1.112 ° for rocking curve measurements showed high quality polycrystalline3C-SiC thin films. Several tendencies regarding the roughness were shown. For Ψ_{high} the roughness/thickness ratio decreased with increasing precursor flow rate, while the opposite trend was observed for Ψ_{low}. A linear dependency of the roughness as a function of the layer thickness for the highest precursor flow rate was detected, while a strong independency for the lowest precursor flow rate was shown. This finding demonstrates the influence of ASD precursor flow rates, indicating different growth mechanism of the SiC crystals. Further investigations to better understand the crystal growth mechanisms are in the focus.

Investigations of the surface properties of three differently terminated 3C-SiC thin films provided prove that one ASD cycle consists of the deposition of an ultra-thin silicon layer and a subsequent carbon-assisted redistribution of the silicon atoms. This cyclic crystal growth mechanism forms smooth and homogenous 3C-SiC thin film. The absence of Si- or C-rich layers in the 3C-SiC thin could be confirmed by HRTEM investigations of the 3C-SiC interface. The impact of ASD parameters on 3C-SiC thin film properties provide to a large extend the possibility to tailor required thin film characteristics depending on the desired MEMS application.

CRediT authorship contribution statement

Ulrich Schmid: Writing – review & editing, Validation, Supervision, Project administration, Funding acquisition, Conceptualization, Methodology, Resources. **Georg Pfusterschmied:** Writing – review & editing, Validation, Supervision, Methodology, Conceptualization, Investigation, Project administration, Resources. **Philipp Moll:** Writing – original draft, Visualization, Methodology, Investigation, Conceptualization, Data curation, Formal analysis, Writing – review & editing. **Michael Stöger-Pollach:** Formal analysis, Investigation, Writing – review & editing, Resources. **Sabine Schwarz:** Formal analysis, Data curation, Investigation, Writing – review & editing.

Declaration of Competing Interest

The authors declare that they have no known competing financial interests or personal relationships that could have appeared to influence the work reported in this paper.

Data Availability

The data that has been used is confidential.

Appendix A. Supporting information

Supplementary data associated with this article can be found in the online version at doi:10.1016/j.sna.2024.115376.

References

[1] A.J. Steckl, C. Yuan, J.P. Li, M.J. Loboda, Growth of crystalline 3C-SiC on Si at reduced temperatures by chemical vapor deposition from silacyclobutane, Appl. Phys. Lett. 63 (24) (1993) 3347–3349, https://doi.org/10.1063/1.110140.

[2] H. Zheng, Z. Fu, B. Lin, X. Li, Controlled-growth and characterization of 3C-SiC and 6H-SiC films on C-plane sapphire substrates by LPCVD, J. Alloy. Compd. 426 (1) (2006) 290–294, https://doi.org/10.1016/j.jallcom.2006.01.094.

[3] Choyke, W.J., H. Matsunami, and G. Pensl, Silicon Carbide: Recent Major Advances. 2004, Switzerland: Springer Nature ISBN: 978-3-642-62333-2.

[4] Y.-M. Zhao, G.-S. Sun, J. Ning, X.-F. Liu, W.-S. Zhao, L. Wang, J.-M. Li, Doped polycrystalline 3C-SiC films deposited by LPCVD for radio-frequency MEMS applications, Chin. Phys. Lett. 25 (6) (2008) 2269. ⟨https://cpl.iphy.ac.cn/Y2008/V25/I6/02269⟩ (URL:).

[5] Shur, M., S. Rumyantsev, and M. Levinshtein, SiC Materials and Devices: Volume I. Vol. 1. 2006, Singapore: World Scientific ISBN: 981-256-835-2.

[6] Shur, M., S. Rumyantsev, and M. Levinshtein, SiC Materials and Devices: Volume II. Vol. 2. 2006, Singapore: World Scienific ISBN: 981-270-383-7.

[7] D. Choi, R.J. Shinavski, W.S. Steffier, S.M. Spearing, Residual stress in thick low-pressure chemical-vapor deposited polycrystalline SiC coatings on Si substrates, J. Appl. Phys. 97 (7) (2005) 074904, https://doi.org/10.1063/1.1866495.

[8] Wijesundara, M.B.J., and R. Azevedo, Silicon Carbide Microsystems for Harsh Environments. 2011, Switzerland: Springer ISBN: 978-1-4419-7120-3.

[9] Y.T. Yang, K.L. Ekinci, X.M.H. Huang, L.M. Schiavone, M.L. Roukes, C.A. Zorman, M. Mehregany, Monocrystalline silicon carbide nanoelectromechanical systems, Appl. Phys. Lett. 78 (2) (2001) 162–164, https://doi.org/10.1063/1.1338959.

[10] S. Nakashima, M. Hangyo, Raman intensity profiles and the stacking structure in SiC polytypes, Solid State Commun. 80 (1) (1991) 21–24, https://doi.org/10.1016/0038-1098(91)90590-R.

[11] Y. Ishida, T. Takahashi, H. Okumura, S. Yoshida, T. Sekigawa, Atomically flat 3C-SiC epilayers by low pressure chemical vapor deposition, Jpn. J. Appl. Phys. 36 (Part 1, No. 11) (1997) 6633–6637, https://doi.org/10.1143/jjap.36.6633.

[12] L. Wang, S. Dimitrijev, J. Han, P. Tanner, A. Iacopi, L. Hold, Demonstration of p-type 3C–SiC grown on 150mm Si(100) substrates by atomic-layer epitaxy at 1000°C, J. Cryst. Growth 329 (1) (2011) 67–70, https://doi.org/10.1016/j.jcrysgro.2011.06.041.

[13] S. Noh, X. Fu, L. Chen, M. Mehregany, A study of electrical properties and microstructure of nitrogen-doped poly-SiC films deposited by LPCVD, Sens. Actuators A Phys. 136 (2) (2007) 613–617, https://doi.org/10.1016/j.sna.2006.12.024.

[14] X.-A. Fu, J.L. Dunning, C.A. Zorman, M. Mehregany, Polycrystalline 3C-SiC thin films deposited by dual precursor LPCVD for MEMS applications, Sens. Actuators A Phys. 119 (1) (2005) 169–176, https://doi.org/10.1016/j.sna.2004.09.009.

[15] M.B.J. Wijesundara, D. Gao, C. Carraro, R.T. Howe, R. Maboudian, Nitrogen doping of polycrystalline 3C-SiC films grown using 1,3-disilabutane in a conventional LPCVD reactor, J. Cryst. Growth 259 (1) (2003) 18–25, https://doi.org/10.1016/S0022-0248(03)01573-2.

[16] X.-A. Fu, R. Jezeski, C.A. Zorman, M. Mehregany, Use of deposition pressure to control residual stress in polycrystalline SiC films, Appl. Phys. Lett. 84 (3) (2004) 341–343, https://doi.org/10.1063/1.1640781.

[17] H. Nagasawa, Y. Yamaguchi, Heteroepitaxial growth of 3C-SiC by LPCVD with alternate gas supply, Amorph. Cryst. Silicon Carbide IV (1992) 40–48, https://doi.org/10.1007/978-3-642-84804-9_5.

[18] H. Phan, P. Tanner, D.V. Dao, L. Wang, N. Nguyen, Y. Zhu, S. DimitrijevPiezoresistive effect of p-type single crystalline 3C-SiC 3 (35 IEEE Electron Device Lett. 2014, ,thinfilm, 53399–401, 10.1109/LED.2014.2301673..

[19] Saddow, S.E., Silicon Carbide Materials for Biomedical Applications. Silicon Carbide Biotechnology, ed. S.E. Saddow. 2016, Oxford: Elsevier ISBN: 978-0-12-802993-0.

[20] Saddow, S.E., Silicon Carbide Biotechnology. A Biocompatible Semiconductor for Advanced Biomedical Devices and Applications. Silicon Carbide Biotechnology, ed. S.E. Saddow. 2012, Oxford: Elsevier ISBN: 978-0-12-385906-8.

[21] J.A. Powell, L.G. Matus, M.A. Kuczmarski, Growth and characterization of cubic SiC single-crystal films on Si, J. Electrochem. Soc. 134 (6) (1987) 1558–1565, https://doi.org/10.1149/1.2100708.

[22] H. Nagasawa, K. Yagi, 3C-SiC single-crystal films grown on 6-inch Si substrates, Phys. Status Solidi (b) 202 (1) (1997) 335–358, https://doi.org/10.1002/1521-3951(199707)202:1<335::AID-PSSB335>3.0.CO;2-Y.

[23] G. Krötz, H. Möller, M. Eickhoff, S. Zappe, R. Ziermann, E. Obermeier, J. Stoemenos, Heteroepitaxial growth of 3C-SiC on SOI for sensor applications, Mater. Sci. Eng. B 61-62 (1999) 516–521, https://doi.org/10.1016/S0921-5107(98)00464-4.

[24] L. Wang, S. Dimitrijev, J. Han, A. Iacopi, L. Hold, P. Tanner, H.B. Harrison, Growth of 3C–SiC on 150-mm Si(100) substrates by alternating supply epitaxy at 1000°C, Thin Solid Films 519 (19) (2011) 6443–6446, https://doi.org/10.1016/j.tsf.2011.04.224.

[25] J. Trevino, F. Xiao-An, M. Mehregany, C. Zorman, Low-stress, heavily-doped polycrystalline silicon carbide for MEMS applications, 18th IEEE Int. Conf. Micro Electro Mech. Syst. (2005) 451–454, https://doi.org/10.1109/MEMSYS.2005.1453964.

[26] C. Roper, C.C.H.R, R. Maboudian, Silicon carbide thin films using 1,3-disilabutane single precursor for MEMS applications-a review, ECS Trans. 3 (2006) 267, https://doi.org/10.1149/1.2357267.

[27] J. Zhang, R.T. Howe, M. R, Electrical characterization of n-type polycrystalline 3C-silicon carbide thin film deposited by 1,3-disilabutane, J. Electrochem. Soc. 153 (6) (2006) G548, https://doi.org/10.1149/1.2188327.

[28] J.D. Reddy, A.A. Volinsky, C.L. Frewin, C. Locke, S.E. Saddow, Mechanical properties of 3C-SiC films for MEMS applications, MRS Online Proc. Libr. 1049 (2007) 1049-AA03-06, https://doi.org/10.1557/PROC-1049-AA03-06.

[29] B. Bhushan, V.N. Koinkar, Microtribological studies of doped single-crystal silicon and polysilicon films for MEMS devices, Sens. Actuators A Phys. 57 (2) (1996) 91–102, https://doi.org/10.1016/S0924-4247(97)80099-4.
[30] J. Vanhellemont, A.K. Swarnakar, O. Van der Biest, Temperature Dependent Young's Modulus of Si and Ge, ECS Trans. 64 (11) (2014) 283, https://doi.org/10.1149/06411.0283ecst.
[31] K. Shirai, Temperature dependence of young's modulus of silicon, Jpn. J. Appl. Phys. 52 (8R) (2013) 088002, https://doi.org/10.7567/JJAP.52.088002.
[32] M. Pozzi, M. Hassan, A.J. Harris, J.S. Burdess, L. Jiang, K.K. Lee, R. Cheung, G. J. Phelps, N.G. Wright, C.A. Zorman, M. Mehregany, Mechanical properties of a 3C-SiC film between room temperature and 600 °C, J. Phys. D Appl. Phys. 40 (11) (2007) 3335–3342, https://doi.org/10.1088/0022-3727/40/11/012.
[33] X.Y. Song, S. Rajgopal, J.M. Melzak, C.A. Zorman, M. Mehregany, Development of a multilayer SiC surface micromachining process with capabilities and design rules comparable to conventional polysilicon surface micromachining, Mater. Sci. Forum 389-393 (2002) 755–758, https://doi.org/10.4028/www.scientific.net/MSF.389-393.755.
[34] M. Eickhoff, H. Möller, M. Rapp, G. Kroetz, Selective growth of high-quality 3C-SiC using a SiO2 sacrificial-layer technique, Thin Solid Films 345 (2) (1999) 197–199, https://doi.org/10.1016/S0040-6090(99)00233-3.
[35] G. Deokar, M. D'Angelo, C.D. Cavellin, Synthesis of 3C-SiC nanocrystals at the SiO2/Si interface by CO2 thermal treatment, J. Nanosci. Nanotechnol. 11 (10) (2011) 9232–9236, https://doi.org/10.1166/jnn.2011.4286.
[36] E. Hurtós, J. Rodríguez-Viejo, Residual stress and texture in poly-SiC films grown by low-pressure organometallic chemical-vapor deposition, J. Appl. Phys. 87 (4) (2000) 1748–1758, https://doi.org/10.1063/1.372087.
[37] F. Lloret, J. Piñero, D. Araujo, M.P. Villar, E. Gheeraert, A. Vo-Ha, V. Soulière, M. Rebaud, D. Carole, G. Ferro, Diamond as substrate for 3C-SiC growth: A TEM study (p. n/a-n/a), Phys. Status Solidi (a) (2014), https://doi.org/10.1002/pssa.201431179.
[38] V. Papaioannou, H. Möller, M. Rapp, L. Vogelmeier, M. Eickhoff, G. Krötz, J. Stoemenos, The evolution of cavities in Si at the 3C-SiC/Si interface during 3C-SiC deposition by LPCVD, Mater. Sci. Eng. B 61-62 (1999) 539–543, https://doi.org/10.1016/S0921-5107(98)00469-3.
[39] M. Fanton, D. Snyder, B. Weiland, R. Cavalero, A. Polyakov, M. Skowronski, H. Chung, Growth of nitrogen-doped SiC boules by halide chemical vapor deposition, J. Cryst. Growth 287 (2) (2006) 359–362, https://doi.org/10.1016/j.jcrysgro.2005.11.044.
[40] M. Yazdanfar, H. Pedersen, P. Sukkaew, I.G. Ivanov, Ö. Danielsson, O. Kordina, E. Janzén, On the use of methane as a carbon precursor in chemical vapor deposition of silicon carbide, J. Cryst. Growth 390 (2014) 24–29, https://doi.org/10.1016/j.jcrysgro.2013.12.033.
[41] M. Zielinski, P.M.C.T.J.S, H. Peyre, Nitrogen doping of 3C-SiC thin films grown by CVD in a resistively heated horizontal hot-wall reactor, J. Cryst. Growth 310 (13) (2008) 3174, https://doi.org/10.1016/j.jcrysgro.2008.03.022.
[42] C.A. Zorman, S. Rajgopal, X.A. Fu, R. Jezeski, J. Melzak, M. M, Deposition of polycrystalline 3C-SiC films on 100 mm diameter Si(100) wafers in a large-volume LPCVD furnace, Electrochem. Solid State Lett. 5 (10) (2002) G99, https://doi.org/10.1149/1.1506461.
[43] L. Wang, S. Dimitrijev, A. Fissel, G. Walker, J. Chai, L. Hold, A. Fernandes, N.-T. Nguyen, A. Iacopi, Growth mechanism for alternating supply epitaxy: the unique pathway to achieve uniform silicon carbide films on multiple large-diameter silicon substrates, RSC Adv. 6 (20) (2016) 16662–16667, https://doi.org/10.1039/C5RA24797G.
[44] T. Shimizu, Y. Ishikawa, N. Shibata, Epitaxial growth of 3C-SiC on thin silicon-on-insulator substrate by chemical vapor deposition using alternating gas supply, Jpn. J. Appl. Phys. 39 (Part 2, No. 6B) (2000) L617–L619, https://doi.org/10.1143/jjap.39.l617.
[45] H. Nagasawa, Y. Yamaguchi, Atomic level epitaxy of 3C-SiC by low pressure vapour deposition with alternating gas supply, Thin Solid Films 225 (1) (1993) 230–234, https://doi.org/10.1016/0040-6090(93)90160-Q.
[46] J.-J. Huang, C. Militzer, C.A. Wijayawardhana, U. Forsberg, H. Pedersen, Superconformal silicon carbide coatings via precursor pulsed chemical vapor deposition, J. Vac. Sci. Technol. A 41 (3) (2023) 030403, https://doi.org/10.1116/6.0002461.
[47] P. Moll, G. Pfusterschmied, U. Schmid, Robust polycrystalline 3C-Sic-on-Si heterostructures with low CTE mismatch up to 900 °C for MEMS, IEEE 36th Int. Conf. Micro Electro Mech. Syst. (MEMS) 2023 (2023) 590–593, https://doi.org/10.1109/MEMS49605.2023.10052144.
[48] P. Becker, P. Scyfried, H. Siegert, The lattice parameter of highly pure silicon single crystals, Z. F. üR. Phys. B Condens. Matter 48 (1) (1982) 17–21, https://doi.org/10.1007/BF02026423.
[49] N. Bécourt, J.L. Ponthenier, A.M. Papon, C. Jaussaud, Influence of temperature on the formation by reactive CVD of a silicon carbide buffer layer on silicon, Wide-band-Gap Semicond. (1993) 79–84, https://doi.org/10.1016/B978-0-444-81573-6.50012-8.
[50] M. Bosi, G. Attolini, M. Negri, C. Frigeri, E. Buffagni, C. Ferrari, T. Rimoldi, L. Cristofolini, L. Aversa, R. Tatti, R. Verucchi, Optimization of a buffer layer for cubic silicon carbide growth on silicon substrates, J. Cryst. Growth 383 (0)) (2013) 84–94, https://doi.org/10.1016/j.jcrysgro.2013.08.005.
[51] G. Ferro, Y. Monteil, H. Vincent, V. Thevenot, M.D. Tran, F. Cauwet, J. Bouix, Atomic force microscopy growth modeling of SiC buffer layers on Si(100) and quality optimization, J. Appl. Phys. 80 (8) (1996) 4691–4702, https://doi.org/10.1063/1.363453.
[52] C.J. Mogab, H.J. Leamy, Conversion of Si to epitaxial SiC by reaction with C2H2, J. Appl. Phys. 45 (3) (1974) 1075–1084, https://doi.org/10.1063/1.1663370.
[53] Z. Zhao, Y. Li, Z. Yin, Z. Li, Growth of 3C-SiC on Si(100) by LPCVD using a modified process after the clean step, J. Mater. Sci.: Mater. Electron. 27 (7) (2016) 7095–7099, https://doi.org/10.1007/s10854-016-4670-7.
[54] S. Roy, M. Portail, T. Chassagne, J.M. Chauveau, P. Vennéguès, M. Zielinski, Transmission electron microscopy investigation of microtwins and double positioning domains in (111) 3C-SiC in relation with the carbonization conditions (p.), Appl. Phys. Lett. 95 (8) (2009), https://doi.org/10.1063/1.3202783.
[55] J.-J. Huang, C. Militzer, C. Wijayawardhana, U. Forsberg, L. Ojamäe, H. Pedersen, Controlled CVD growth of highly ⟨111⟩-oriented 3C-SiC, J. Phys. Chem. C 126 (23) (2022) 9918–9925, https://doi.org/10.1021/acs.jpcc.2c01171.
[56] M.J.P. Duchemin, M.M. Bonnet, M.F. Koelsch, Kinetics of silicon growth under low hydrogen pressure, J. Electrochem. Soc. 125 (4) (1978) 637, https://doi.org/10.1149/1.2131515.
[57] F. Hottier, R. Cadoret, Surface processes in low pressure chemical vapour deposition, J. Cryst. Growth 52 (1981) 199–206, https://doi.org/10.1016/0022-0248(81)90194-9.
[58] W. Weerts, M. De Croon, G. Marin, The kinetics of the low-pressure chemical vapor deposition of polycrystalline silicon from silane, J. Electrochem. Soc. 145 (4) (1998) 1318, https://doi.org/10.1149/1.1838458.
[59] B.L. Sopori, X. Deng, J.P. Benner, A. Rohatgi, P. Sana, S.K. Estreicher, Y.K. Park, M. A. Roberson, hydrogen in silicon: a discussion of diffusion and passivation mechanisms, Sol. Energy Mater. Sol. Cells 41-42 (1996) 159–169, https://doi.org/10.1016/0927-0248(95)00098-4.
[60] T. Tezuka, N. Hirashita, Y. Moriyama, N. Sugiyama, K. Usuda, E. Toyoda, K. Murayama, S.-i Takagi, {110}-facets formation by hydrogen thermal etching on sidewalls of Si and strained-Si fin structures, Appl. Phys. Lett. 92 (19) (2008) 191903, https://doi.org/10.1063/1.2924281.
[61] R.J. Iwanowski, K. Fronc, W. Paszkowicz, M. Heinonen, XPS and XRD study of crystalline 3C-SiC grown by sublimation method, J. Alloy. Compd. 286 (1) (1999) 143–147, https://doi.org/10.1016/S0925-8388(98)00994-3.
[62] C. Locke, C.L. Frewin, J. Wang, S.E. Saddow, Growth of single crystal 3C-SiC(111) on a poly-Si seed layer, Mater. Sci. Forum 615-617 (2009) 157–160, https://doi.org/10.4028/www.scientific.net/MSF.615-617.157.
[63] H. Zheng, J. Su, Z. Fu, G. Li, X. Li, Heteroepitaxial growth and characterization of 3C-SiC films on-axis si (110) substrates by LPCVD, Ceram. Int. 34 (3) (2008) 657–660, https://doi.org/10.1016/j.ceramint.2007.02.011.
[64] T. Nishiguchi, M. Nakamura, K. Nishio, T. Isshiki, S. Nishino, Heteroepitaxial growth of (111) 3C–SiC on well-lattice-matched (110) Si substrates by chemical vapor deposition, Appl. Phys. Lett. 84 (16) (2004) 3082–3084, https://doi.org/10.1063/1.1719270.
[65] X.A. Fu, J.L. Dunning, C.A. Zorman, M. Mehregany, Polycrystalline 3C-SiC thin films deposited by dual precursor LPCVD for MEMS applications, Sens. Actuators 119 (1) (2005) 169, https://doi.org/10.1016/j.sna.2004.09.009.
[66] E. Hurtos, J. Rodrıguez-Viejo, Residual stress and texture in poly-SiC films grown by low-pressure organometallic chemical-vapor deposition, J. Appl. Phys. 87 (4) (2000) 1748–1758, https://doi.org/10.1063/1.372087.
[67] H. Kikuchi, R.K. Kalia, A. Nakano, P. Vashishta, P.S. Branicio, F. Shimojo, Brittle dynamic fracture of crystalline cubic silicon carbide (3C-SiC) via molecular dynamics simulation, J. Appl. Phys. 98 (10) (2005) 103524, https://doi.org/10.1063/1.2135896.
[68] G.-S. Chung, K.-S. Kim, Characteristics of poly-crystalline 3C-SiC thin films grown for micro/nano-electromechanical systems by using single-precursor hexamethyldisilane, J. Korean Phys. Soc. 51 (4) (2007) 1389–1394, https://doi.org/10.3938/jkps.51.1389.
[69] P. Moll, G. Pfusterschmied, M. Schneider, M. Dorfmeister, S. Knafl, H. D. Wanzenboeck, U. Schmid, Biocompatible a-SiC:H-based bistable MEMS membranes with piezoelectric switching capability in fluids, J. Micro Syst. 31 (3) (2022) 372–383, https://doi.org/10.1109/JMEMS.2022.3163477.
[70] V. Silverio, P.A.G. Canane, S. Cardoso, Surface wettability and stability of chemically modified silicon, glass and polymeric surfaces via room temperature chemical vapor deposition, Colloids Surf. A Physicochem. Eng. Asp. 570 (2019) 210–217, https://doi.org/10.1016/j.colsurfa.2019.03.032.
[71] Y. Xiang, P. Fulmek, D. Platz, U. Schmid, Temperature dependence of water contact angle on teflon AF1600, Langmuir 38 (4) (2022) 1631–1637, https://doi.org/10.1021/acs.langmuir.1c03202.
[72] F. Lukeš, Oxidation of Si and Ga-As in air at room temperature, Surf. Sci. 30 (1) (1972) 91–100, https://doi.org/10.1016/0039-6028(72)90025-8.
[73] V. Presser, K.G. Nickel, Silica on silicon carbide, Crit. Rev. Solid State Mater. Sci. 33 (1) (2008) 1–99, https://doi.org/10.1080/10408430701718914.
[74] I. Vickridge, J. Ganem, Y. Hoshino, I. Trimaille, Growth of SiO2 on SiC by dry thermal oxidation: mechanisms, J. Phys. D Appl. Phys. 40 (20) (2007) 6254, https://doi.org/10.1088/0022-3727/40/20/S10.
[75] M. Schnabel, E. Arca, Y. Ha, C. Stetson, G. Teeter, S.-D. Han, P. Stradins, Enhanced interfacial stability of Si anodes for Li-ion batteries via surface SiO2 coating, ACS Appl. Energy Mater. 3 (9) (2020) 8842–8849, https://doi.org/10.1021/acsaem.0c01337.
[76] L. Muehlhoff, M.J. Bozack, W.J. Choyke, J.T. Yates Jr., Comparative oxidation studies of SiC(0001¯) and SiC(0001) surfaces, J. Appl. Phys. 60 (7) (1986) 2558–2563, https://doi.org/10.1063/1.337121.
[77] V. Šimonka, A. Hössinger, J. Weinbub, S. Selberherr, Growth rates of dry thermal oxidation of 4H-silicon carbide, J. Appl. Phys. 120 (13) (2016) 135705, https://doi.org/10.1063/1.4964688.

Philipp Moll moved to Vienna in 2012, when he started his study in Electrical Engineering at TU Wien. During his studies he worked at Hellpower, a batterie pack manufacturer until 2020, when he finished his master degree in Biomedical Engineering, specialized in Signals and Instrumentation. The final thesis was about bistable switching of biocompatible SiC MEMS membranes in fluids, which successfully led to continuing his academic career with a position as a PhD student at the Institute for Sensors and Actuator Systems at TU Wien, researching polycrystalline 3 C SiC thin films. Studying this topic from 2020 to 2024 included basic of research of thin film formation using low pressure vapor chemical depositions, contact formation on poly SiC thin films or the electrical characterization of highly doped 3C-SiC using a novel deposition approach with the alternating supply deposition technique. Eventually, with the gathered knowledge he fabricated a 3C-SiC-based micro hotplate for MEMS applications.

Dr. Georg Pfusterschmied studied material science at TU Wien. In 2014, he started his PhD thesis in the field of microsystems technology at ISAS/TU Wien. During his PhD, he focused on designing, manufacturing and characterization of piezoelectric MEMS resonators for viscosity and density characterization of fluids. In the process of his PhD thesis, he was also a visiting researcher at John Sader's research group at the School of Mathematics and Statistics at University of Melbourne. His PhD thesis was awarded with the Lions Award in 2016 and the Dr. Fehrer Award in 2019. After defending his thesis in 2018, Dr Pfusterschmied continued his research at ISAS, focusing on SiC Technology.

Sabine Schwarz studied Technical Physics at TU Wien from 1996 to 2002, completing her PhD in 2005. Her involvement in Transmission Electron Microscopy commenced as early as 2000 during her studies. Her doctoral research focused on investigating the precipitation structure of SmCo 2:17 magnets, followed by further research on the microstructure and magnetic reversal of advanced recording media. From 2005–2007, she worked at the Austrian Research Centers in Seibersdorf, primarily investigating the microstructure of steel. She returned to university in 2007 until now as a researcher specializing in electron microscopy studies, with a primary focus on materials science. In this role, she conducts contract research for both students and external clients, as well as providing training for students on various microscope techniques.

Dr. Michael Stöger-Pollach is working as professor for electron microscopy at the TU Wien. He received his PhD in physics at TU Wien, Austria, in 2004. His research interest are electron energy loss spectrometry in the transmission electron microscope, optical properties of semiconductors, band gap determination and relativistic effects in valence electron energy loss spectrometry. He is General Sectretry of the Austrian Society for Electron Microscopy (ASEM).

Prof. Dr. U. Schmid started studies in physics at the University of Kassel in 1992. He performed his diploma work at the research laboratories of Daimler-Benz AG (now: Mercedes-Benz Group) on the electrical characterization of silicon carbide microelectronic devices. In 1999, he joined the research laboratories of EADS GmbH (now: Airbus Group) in Ottobrunn/Munich, Germany. From 2003–2008, he was Post-doc at the Chair of Micromechanics, Microfluidics/Microactuators at Saarland University. Since October 2008, he is full professor for Microsystems Technology at TU Wien heading since 2012 the Institute of Sensor and Actuator Systems. U. Schmid has authored or co-authored more than 450 peer-reviewed publications in journals and international conferences and holds more than 55 different granted patent families.